New Phytologist

Modelling optimal ligninolytic activity during plant litter decomposition

Arjun Chakrawal[1], **Björn D. Lindahl**[2] **and Stefano Manzoni**[1]

[1]Department of Physical Geography and Bolin Centre for Climate Research, Stockholm University, 10691, Stockholm, Sweden; [2]Swedish University of Agricultural Sciences, Department of Soil and Environment, 75007, Uppsala, Sweden

Author for correspondence:
Arjun Chakrawal
Email: arjun.chakrawal@natgeo.su.se

Received: *11 October 2023*
Accepted: *22 January 2024*

New Phytologist (2024) **243:** 866–880
doi: 10.1111/nph.19572

Key words: aromatic, eco-evolutionary dynamics, lignin, litter decomposition, metabolic tradeoff, optimal control.

Summary

- A large fraction of plant litter comprises recalcitrant aromatic compounds (lignin and other phenolics). Quantifying the fate of aromatic compounds is difficult, because oxidative degradation of aromatic carbon (C) is a costly but necessary endeavor for microorganisms, and we do not know when gains from the decomposition of aromatic C outweigh energetic costs.
- To evaluate these tradeoffs, we developed a litter decomposition model in which the aromatic C decomposition rate is optimized dynamically to maximize microbial growth for the given costs of maintaining ligninolytic activity. We tested model performance against >200 litter decomposition datasets collected from published literature and assessed the effects of climate and litter chemistry on litter decomposition.
- The model predicted a time-varying ligninolytic oxidation rate, which was used to calculate the lag time before the decomposition of aromatic C is initiated. Warmer conditions increased decomposition rates, shortened the lag time of aromatic C oxidation, and improved microbial C-use efficiency by decreasing the costs of oxidation. Moreover, a higher initial content of aromatic C promoted an earlier start of aromatic C decomposition under any climate.
- With this contribution, we highlight the application of eco-evolutionary approaches based on optimized microbial life strategies as an alternative parametrization scheme for litter decomposition models.

Introduction

The question of whether the decomposition of complex polymers, such as lignin and similar compounds, represents a significant rate-limiting step to terrestrial carbon (C) cycling has been a subject of extensive research. However, a gap in understanding of the mechanistic controls on the decomposition of these recalcitrant compounds remains (Thevenot *et al.*, 2010; Hall *et al.*, 2020). Plant detritus, exudates, and their derived compounds are building blocks of particulate and mineral-associated organic matter (Huang *et al.*, 2019; Cotrufo & Lavallee, 2022). Therefore, accurate predictions of decomposition rates of these litter components are crucial for better understanding the fate of C in soils (Moorhead & Sinsabaugh, 2006). Moreover, litter decomposition releases essential plant nutrients, and in some ecosystems, low decomposition rates contribute to retention of nutrients in recalcitrant pools. However, the timing of lignin decomposition, the associated release of lignin-protected compounds, and the tradeoffs with other microbial functions are not well understood, leaving uncertainties regarding incorporation of litter-derived organic matter into the soil and nutrient release during decomposition. Much of the lignin is released as CO_2 during decomposition as mainly basidiomycete fungi degrade it to get access to energy and nutrient-rich compounds, and part of it may also be used to fuel fungal growth (Berg & McClaugherty, 1987; Kirk & Farrell, 1987; del Cerro *et al.*, 2021). In particular, uncertainty surrounding the temperature sensitivity of decomposition rates of lignin-like compounds in aboveground litter, topsoil, and subsoil hinders our capacity to quantify the persistence of soil organic C in future warming scenarios (Allison *et al.*, 2018; Chen *et al.*, 2020; Tan *et al.*, 2020; Dao *et al.*, 2022; Zosso *et al.*, 2023).

Much of the uncertainties in assessing the dynamics of lignin decomposition are associated with unknown constraints on fungal communities with ligninolytic capacities. Vivelo & Bhatnagar (2019) suggested that 'decomposer fungal succession is partially rooted in fungal decomposers' deep evolutionary history', implying that microbial activity might be regulated according to evolutionary pressures toward improved fitness. Indeed, the succession of different microbial groups linked to different extracellular enzyme activities is correlated with mass loss of different litter fractions, suggesting that different microbial guilds contribute to the degradation of complex compounds (Šnajdr *et al.*, 2011; Bhatnagar *et al.*, 2018). These community composition dynamics are shaped by microbial succession linked to litter chemical traits (specifically nutrient content and the abundance of recalcitrant compounds) and their interaction with local soil conditions. Together, litter quality and soil properties modulate the activities of community members in controlling litter decomposition (Buresova *et al.*, 2019; Herzog *et al.*, 2019). Additionally, extracellular enzyme activities change during litter decomposition, even when litter is colonized by a single fungus (Barbi *et al.*, 2020). Thus, decomposition is regulated by both community-level changes and the dynamic behavior of single organisms. Therefore, developing a conceptual framework that links microbial adaptation to local environmental conditions is essential to disentangle the chemical, physiological, and ecological drivers of litter decomposition rates.

While evolution acts at the species level, our aim here is to develop a pragmatic approach for modelling complex microbial community dynamics with a minimal—albeit ecologically meaningful – set of assumptions. Furthermore, ecological and evolutionary drivers interact in regulating microbial functions by shaping community composition, motivating the study of eco-evolutionary dynamics (Loreau *et al.*, 2023; Martiny *et al.*, 2023). Models based on community-level optimality criteria have been successful in predicting scaling relations between enzyme activities and soil organic matter content at steady state (Calabrese *et al.*, 2022), as well as the relationship between microbial C-use efficiency and nutrient availability (Manzoni *et al.*, 2017). Optimal control theory has been used for investigating the temporal dynamics of decomposition (Manzoni *et al.*, 2023). However, these approaches have not yet been tested in litter decomposition models where different chemical compounds interact nonlinearly, such as in the case of lignin, which may protect high-energy compounds from decomposition by complex formation.

Optimal control theory attempts to find the optimal temporal trajectory of a model parameter (i.e. the 'control' variable), which maximizes a given goal function. A classic example is the partition of photosynthate into vegetative growth and reproduction with the goal of maximizing seed yield (King & Roughgarden, 1982). In this contribution, we formulated an eco-evolutionary model built on the assumption that the ligninolytic activity of the litter-decomposing community is dynamic and adapted to maximize the collective community fitness. Mathematically, this means optimizing ligninolytic activity through time to maximize the mean microbial growth rate throughout the decomposition process.

Such an optimization approach is appropriate because it allows the balancing of the costs and benefits of lignin degradation. The main benefit is access to substrates otherwise protected by the complex organic structure and complexations of lignin. The main cost is related to the maintenance of oxidative enzymes. Fungal oxidation of unhydrolysable compounds, including lignin, has been described as 'enzymatic combustion' (Kirk & Farrell, 1987) – an energetically costly process (Shimizu *et al.*, 2005; Moorhead *et al.*, 2013), as it relies on continuous generation of hydrogen peroxide by the fungi to be used as an electron acceptor (Mattila *et al.*, 2022). Oxidative degradation facilitates increased access to, for example cellulose and proteins, which are often protected from hydrolysis by interactions with lignin, tannins, melanin, and other unhydrolysable compounds (Berg & McClaugherty, 1987; Kirk & Farrell, 1987). It can then be hypothesized that if oxidation is costly, it should not be initiated until 'lignin-free' hydrolysable compounds are depleted. Therefore, we expect our model to predict optimal lignin decomposition to start earlier in litter with initially high lignin content, or when warmer conditions promote fast microbial consumption of lignin-free compounds.

We developed and tested a minimalist model of litter decomposition that follows organic C into two pools – nonaromatic C and aromatic C. Building on the optimal control framework developed by Manzoni *et al.* (2023), we use the mean microbial growth rate as a proxy for microbial fitness to predict the optimal ligninolytic strategy. Specifically, we answer the following questions:

(**1**) Does this eco-evolutionary approach have more predictive power than a model with time-invariant rate parameters?

(**2**) Is climate or litter chemistry the more dominant control on ligninolytic oxidation rate?

(**3**) How does the investment in ligninolytic and hydrolytic enzymes change with climate and litter chemical traits?

Materials and Methods

We start by describing a two-pool litter decomposition model (Litter decomposition model section). Next, Data collation and preparation section describes the data collected from published sources used in model parametrization. The eco-evolutionary approach is described in Eco-evolutionary approach: litter decomposition as an optimal control problem section and the least-square fitting in Least-square model-data fitting section. Finally, Statistical analyses section explains the linear mixed-effect models used to identify relationships between estimated model parameters and climatic and litter chemical traits.

Litter decomposition model

We developed a litter decomposition model that describes the interactions between litter chemistry and microbial traits. The model was parametrized using mass (or C) and lignin loss data from litter bag incubations in field conditions. 'Lignin' is here defined as acid unhydrolysable residues (AURs) corrected to account for measurement bias, and including both lignin and similar aromatic compounds, such as tannins and other polyphenols.

In the model, we divide litter C into a nonaromatic C pool (C_{H}, expressed as g of C in the modelled domain, e.g. a litterbag), dominated by polymers susceptible to hydrolytic enzymes, including cellulose and hemicellulose, and an aromatic C pool (C_{O}, also expressed as g of C), representing aromatic C in lignin and condensed tannins that require oxidative ligninolytic enzymes for their decomposition (Fig. 1a). The nonaromatic pool contains both nonaromatic constituents of aromatic compounds and nonaromatic compounds that are unhydrolysable because they are complex-bound to aromatic compounds. This implies that the two pools do not decompose independently. Mathematically, the protection of nonaromatic C by aromatic C in lignocellulose complexes is simulated using a factor p, which reduces the decomposition rate of the nonaromatic pool with

New Phytologist

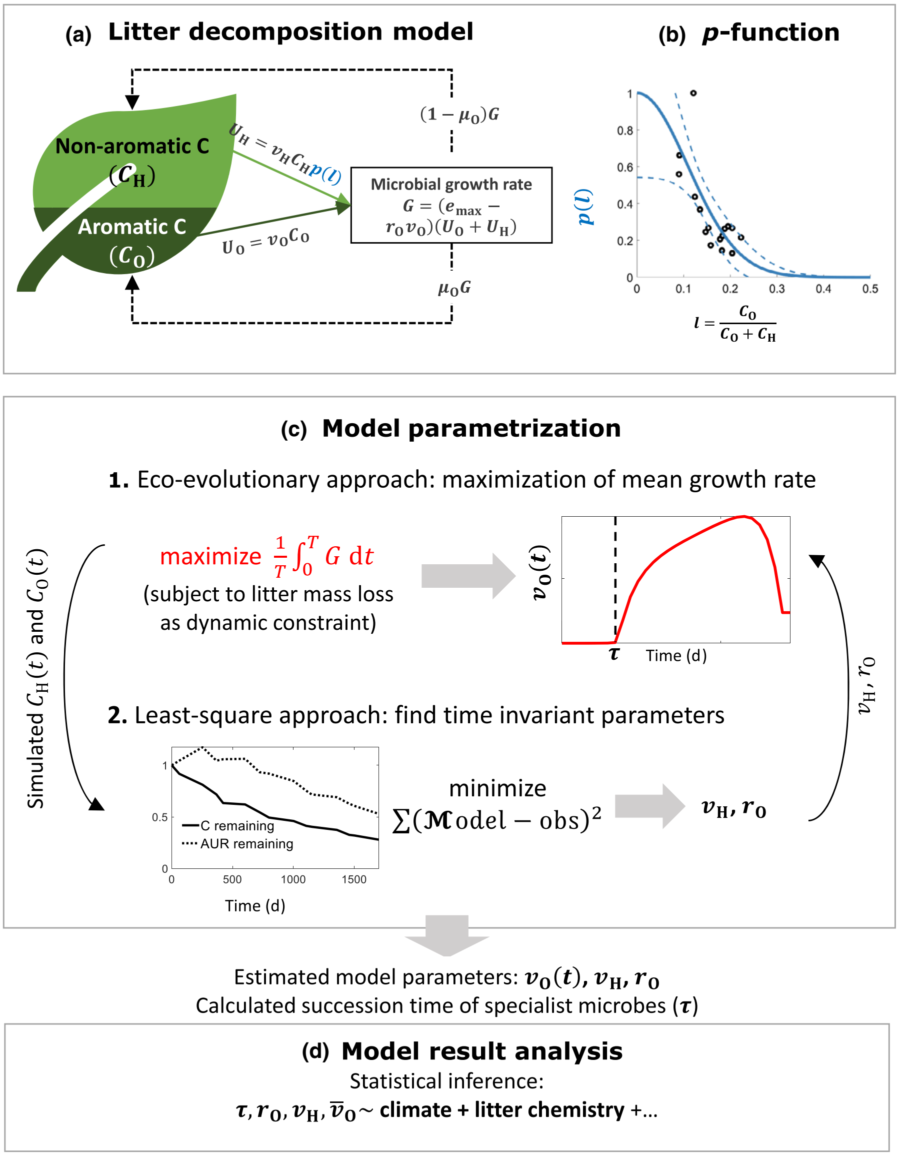

Fig. 1 Schematic of (a) litter decomposition model, (b) reduction in the hydrolytic rate (v_H) due to the presence of aromatic carbon, as represented by the function $p(l)$ (solid line), where l is the fraction of aromatic carbon (C) in the litter (Eqn 1), (c) model parametrization scheme including the eco-evolutionary approach and data-model fitting, and (d) statistical inference on estimated parameters with climatic variables and litter chemical traits. Data points, obtained from Bonanomi *et al*. (2013), in (b) represent aromatic C obtained from NMR analysis, and p is the calculated (and normalized) rate of decomposition of the nonaromatic C pool. The dashed lines in panel b indicate 95% confidence interval of the scaling parameter a in Eqn 1. The succession time of specialist microbes (e.g. basidiomycete fungi) is the same as ligninolysis lag time.

increasing fraction of aromatic C (Fig. 1b). At low aromatic C contents, this protective effect is negligible, and $p \approx 1$; at aromatic C contents close to 15% (on a total litter C basis), the accessibility to nonaromatic C is approximately halved.

The nonaromatic and aromatic pools are decomposed with first-order kinetics (suitable to describe dynamics at annual or longer scales), in which the rate constants account implicitly for extracellular enzyme activity. The rate constant v_H of the nonaromatic pool is time-invariant, whereas the rate constant v_O of the aromatic pool is assumed to vary through time due to dynamic changes in microbial resource acquisition strategy. For ease of interpretation, we refer to v_H and v_O as the hydrolytic and the ligninolytic oxidation rate, respectively.

We assume that microorganisms can utilize both pools for growth purposes (del Cerro *et al*., 2021); however, their C-use efficiency is at maximum (e_{max}) when the aromatic pool is not used and decreases linearly with increasing v_O due to metabolic cost of producing oxidative enzymes and hydrogen peroxide to sustain oxidation (Manzoni *et al*., 2021). The cost factor is denoted by r_O (expressed in days) and referred to as cost of ligninolytic. Furthermore, we assume a quasi-steady state for the microbial biomass so that the microbial growth rate (G) is equal to mortality. In other words, microbial biomass is not directly modelled, but its effect on decomposition is implicitly described through the values and temporal changes in the kinetic constants. A fraction μ_O of the microbial necromass is recycled into the aromatic pool. A higher value of μ_O indicates that a higher fraction of microbial necromass is of aromatic nature, whereas a lower value indicates that necromass is mostly nonaromatic. With these assumptions, the mass balance equations for the nonaromatic and aromatic pools are written as,

$$\frac{\mathrm{d}C_H}{\mathrm{d}t} = (1-\mu_O)G - v_H C_H p \qquad \text{Eqn 1}$$

$$\frac{dC_O}{dt} = \mu_O G - v_O C_O \quad \text{Eqn 2}$$

where the microbial growth rate is given as the product of C-use efficiency (CUE, ratio of growth over C uptake) and C acquisition rate,

$$G = \mathrm{CUE}(v_H C_H p + v_O C_O) = (e_{\max} - r_O v_O)(v_H C_H p + v_O C_O). \quad \text{Eqn 3}$$

The p-function is formulated as,

$$p = \exp\left(-\left(\frac{l}{a}\right)^2\right) \quad \text{Eqn 4}$$

where $l = C_O/(C_O + C_H)$ and a is a scaling exponent (Fig. 1b). The energetic costs of maintaining the oxidative processes is modelled as a reduction in microbial CUE (Moorhead *et al.*, 2013; Manzoni *et al.*, 2021). Thus, CUE varies through time because of the time-dependent cost of ligninolysis, as $\mathrm{CUE} = e_{\max} - r_O v_O$.

Model parametrization

The model has six parameters: μ_O, $e_{\max}$, v_O, v_H, r_O and a. The fraction of necromass C recycled into aromatic pools μ_O was fixed based on estimates of unhydrolysable content (mainly melanin) of fungal necromass, $\mu_O = 0.1$ (Fernandez *et al.*, 2019; See *et al.*, 2021). A few litter bag samples showed more than a doubling in unhydrolysable C from initial values, possibly due to metabolized C characterized as unhydrolysable residues in the proximate analysis. Such an increase in aromatic C is simulated by assuming a higher fraction of necromass recycled into the aromatic C pool, that is $\mu_O = 0.3$ when fitting the model to data. The maximum growth efficiency $e_{\max}$ was calculated as a function of the initial litter C : N ratio (CN_0) to implicitly account for the effect of nitrogen (N) limitation of microbial growth, $e_{\max} = \min(6.25CN_0^{-0.77}, 0.4)$ (Manzoni *et al.*, 2010). A maximum value of $e_{\max} = 0.4$ was imposed at low CN_0. The ligninolytic oxidation rate, v_O, was estimated dynamically by maximizing the mean microbial growth rate (Eco-evolutionary approach: litter decomposition as an optimal control problem section). The hydrolytic rate, v_H, and the cost of ligninolysis, r_O, are time-invariant parameters estimated by fitting the model to the observed time series of total litter and aromatic C (Least-square model-data fitting section).

The initial mass of aromatic and nonaromatic C was directly set from the observed litter mass loss data. The initial amount of nonaromatic C (gC) was estimated by subtracting the initial amount of aromatic C (gC) from the initial total litter C (gC).

To parameterize the p-function, we utilized 13C NMR spectroscopy data from Bonanomi *et al.* (2013) from a litterbag incubation experiment conducted in Mediterranean and temperate environments. This NMR dataset provided information on the fraction of different functional groups within the total organic C of the litter at four distinct time points: 0, 60, 90, and 180 d. From the NMR data, the fraction of aromatic C was determined by calculating the spectral area under the chemical shift region between 141 and 160 ppm. Since the areas under spectral regions are normalized to 1, the fraction of nonaromatic C is calculated as one minus the fraction of aromatic C. Subsequently, the fractions of aromatic and nonaromatic C were converted into amounts by multiplying them by the remaining C content within the litterbags. Utilizing the amount of nonaromatic C, we computed the first-order rate constants (k) during the initial stage of litter mass loss, specifically within the 0–30 d period. To estimate the scaling coefficient a, we fitted a modified decay function, $k = A\exp\left(-\left(\frac{l}{a}\right)^2\right)$, to these k values as a function of initial fractions of aromatic C l, where A is a normalizing constant. The values of A and a are estimated using least-square fitting. Finally, the p-function is calculated as $p(l) = \frac{k}{A} = \exp\left(-\left(\frac{l}{a}\right)^2\right)$ (Fig. 1b).

Data collation and preparation Litter decomposition data, encompassing total litter mass (or total C) and lignin mass (estimated as Klason lignin, acid detergent lignin, by cupric oxide (CuO) oxidation, or by near-infrared spectroscopy), were compiled from 208 published litter bag datasets from 18 studies (Table 1; Supporting Information Fig. S1). These datasets were digitized directly from the original articles or provided by the authors. Moreover, we did not include studies that indicated significant contributions of abiotic factors to the decomposition of lignin, for example via photodegradation in sites under open canopy and with intense radiation (Méndez *et al.*, 2022), because our model only simulates biotic pathways.

To ensure consistency, we treated Klason lignin, acid detergent lignin, and estimates based on near-infrared spectroscopy as AUR proxies, except for lignin reported using the CuO method (McLellan *et al.*, 1991; Berg & McClaugherty, 2014). NMR spectra have shown that AURs not only encompass most of the aromatic litter constituents, but also contain other organic compounds (Preston & Trofymow, 2015; Baskaran *et al.*, 2019). To convert AUR C into aromatic C, we used NMR spectra of AUR from *Pinus sylvestris L.* litter (Baskaran *et al.*, 2019). By fitting a linear relation between the mass of aromatic C obtained from NMR spectra and that of AUR C from proximate analysis, we determined that 20% of AUR C is aromatic (see Fig. S2). We assumed that this fraction does not change through decomposition and is the same for all litter types, allowing us to convert the time series of measured mass of AUR C to the mass of aromatic C.

Unless reported in the original sources, a 50% C content of litter and 60% C content of AUR (on a dry mass basis) were assumed (Coûteaux *et al.*, 1998; Preston & Trofymow, 2015). No conversion factor was applied to lignin reported using the CuO oxidation method. To calibrate the model to observations, we normalized litter C and aromatic C to their initial values before litterbag incubation. In line with Manzoni *et al.* (2010), for data that exhibited rapid initial C leaching (when the mass at the first measurement point decreased to less than 70% of C_0),

Table 1 Summary of litter decomposition datasets and estimated model parameters.

No.	Study	MAT (°C)	MAP (mm)	Initial CN (g C per gN)	Initial AUR C (g C per g total C)	v_H (d^{-1})	$\overline{v}_O$ (d^{-1})	r_O (d)	τ (d)	Lignin estimation method	Climate	Enzyme activity	Number of incubations
1	Berg & McClaugherty (1989)	3–8	609–799	10–147	0.12–0.50	5.0E-04-2.8E-03	2.5E-04-1.7E-03	6.5–84.2	0–608	Klason	Boreal	na	32
2	Fioretto et al. (2000, 2005, 2007)	19	680	46–62	0.18–0.39	9.5E-04-2.2E-03	9.9E-04-3.6E-03	1.0–17.2	0–163	Acid detergent fiber	Warm Temperate	A	3
3	He et al. (2016)	3	850	26–35	0.28	1.4E-03-1.9E-03	1.4E-03-1.6E-03	16.5–27.4	0–42	Acid detergent fiber	Warm Temperate	na	2
4	He et al. (2019)	12	2100	33–37	0.04–0.09	1.3E-03-2.9E-03	2.4E-03-4.8E-03	3.3–27.0	0	CuO oxidation	Warm Temperate	na	4
5	Hirobe et al. (2004)	26	3850	40–73	0.35–0.62	3.1E-03-1.0E-02	1.8E-03-1.2E-02	0.6–26.3	0–12	Klason	Tropical	na	15
6	Huang et al. (2021)	20	1200	29	0.22	2.4E-03-3.7E-03	3.9E-04-2.2E-03	12.9–26.8	93–208	Acid detergent fiber	Warm Temperate	A	4
7	Kou et al. (2015)	18	1475	36–69	0.18–0.26	1.3E-03-2.1E-03	2.1E-04-6.9E-04	13.5–42.0	124–389	Klason	Warm Temperate	na	9
8	Magill & Aber (1998)	4	1120	42–78	0.20–0.49	5.0E-04-1.5E-03	2.2E-04-1.3E-03	9.8–83.9	0–815	Near-infrared spectroscopy	Cool Temperate	na	18
9	McKee et al. (2016)	13	835	30	0.01	2.1E-03	4.3E-03	1.6	123	Acid detergent fiber	Cool Temperate	na	1
10	Osono (2017)	21	2487	20–110	0.32–0.55	2.1E-03-6.0E-03	8.8E-04-6.8E-03	1.5–36.3	0–232	Klason	Warm Temperate	na	12
11	Osono & Takeda (2005)	10	2495	17–95	0.60	9.6E-04-5.0E-03	5.0E-04-7.2E-03	1.0–113.1	0–203	Klason	Cool Temperate	na	28
12	Preston et al. (2009a,b)	−3 to 7	370–1258	45–1379	0.22–0.51	4.4E-04-1.7E-03	2.1E-04-1.3E-03	7.1–129.0	0–1029	Klason	Cool Temperate	na	15
13	Růžek et al. (2021)	6	1000	53	0.04	1.6E-03-1.8E-03	1.8E-03-2.2E-03	6.5–7.7	0–60	CuO oxidation	Cool Temperate	na	4
14	Šnajdr et al. (2011)	9	647	49	0.49	4.0E-03	2.5E-03	12.7	22	Klason	Cool Temperate	A	1
15	Tu et al. (2011)	16	1490	90–137	0.22–0.32	1.2E-03-4.0E-03	1.4E-03–7.1E-03	0.5–5.9	0–113	Acid detergent fiber	Warm Temperate	na	12
16	Tu et al. (2014)	16	1822	20–265	0.18–0.46	1.4E-03-6.9E-03	1.4E-03-1.2E-02	0.5–16.3	0–140	Acid detergent fiber	Warm Temperate	na	40
17	Yue et al. (2016)	3	850	13–60	0.37–0.60	2.8E-03-1.1E-02	1.1E-03-1.3E-02	2.4–29.1	0–67	Acid detergent fiber	Cool Temperate	na	4
18	Zhou et al. (2017)	16	1772	52	0.22	2.9E-03-3.7E-03	1.5E-03-2.9E-03	9.2–19.4	138–216	Acid detergent fiber	Warm Temperate	na	4

$\overline{v}_O$, mean rate constant of aromatic pool; r_O, cost of ligninolytic enzyme production; v_H, rate constant of nonaromatic pool; A, enzyme activity available; CN, C-to-N ratio; MAP, mean annual precipitation; MAT, mean annual temperature; na, enzyme activity not available; τ, lag time of ligninolytic enzyme, Number of incubations are the observations available. One set of observations is total C and AUR loss time series data.

the initial data point was excluded. Furthermore, we applied a $(C_t - C_{t-1})/C_{t-1} > 0.1$ threshold to remove data points that implied increases in litter mass possibly caused by contamination from external sources.

Eco-evolutionary approach: litter decomposition as an optimal control problem Following Manzoni *et al.* (2023), we formulated litter decomposition as an optimal control problem where we assumed that the microbial community maximizes its mean growth rate over the entire decomposition period (T) by adapting ligninolytic oxidation. The maximization objective (J) can be written as,

$$J = \frac{1}{T}\int_0^T G\mathrm{d}t \qquad \text{Eqn 5}$$

This maximization is constrained by the mass balance Eqns 1 and 2 and constitutes a fixed terminal time and free terminal state problem (Lenhart & Workman, 2007). In other words, the outcome of this optimization problem is an optimal variation in v_{O} that maximizes microbial growth rate in the specified period of time T for a given initial litter chemistry (Fig. 1c).

In principle, the period during which microorganisms maximize their growth can also be optimized. These problems are referred to as free terminal time problems in the literature on optimal control and are numerically more challenging to solve. To keep the problem numerically tractable, we defined the decomposition period as the time when half the mass remaining at the last litter bag harvest was attained. This time was calculated by fitting a single exponential model to litter mass loss data. This procedure only provides the terminal time for the optimization and does not imply that the modelled decomposition trajectories are exponential.

The optimal control problem was solved with numerical methods based on direct collocation, using the Yop toolbox in MATLAB (Leek, 2016).

Least-square model-data fitting We determined the time-invariant parameters v_{H} and r_{O} by least-square fitting of the model output to the time series of total litter C and aromatic C (Fig. 1c). Briefly, we initialized the least-square solver with a guess of v_{H} and r_{O} and then ran the optimal control problem to obtain an estimate of the optimal v_{O} and the temporal dynamics of the state variables C_{H} and C_{O}. The optimal v_{O} was recalculated at each iteration of the least-square solver. Subsequently, we compared the sum of C_{H} and C_{O} with the measured total litter C, and C_{O} with the measured aromatic C using a mean square error metric. To obtain the best-fitted parameters for each litter bag dataset, we employed the MATLAB *lsqcurvefit* function. We used the coefficient of determination (r^2) and the root mean squared error (rmse) to evaluate model performance.

Additionally, for comparison with the optimally controlled v_{O} model, we also fitted the same model (Eqns 1, 2) to the same data but with time-invariant v_{O}. This simpler model version is formally similar to conventional litter decomposition (or soil C) models with fixed parameters. Finally, using a Bayesian information criterion, we compared the predictive accuracy of these two models.

Statistical analyses

Using the best-fitted parameters, we estimated the ligninolysis lag time (τ) as the time when v_{O} increased above 5% of the maximum value (i.e. at the threshold $v_{\mathrm{O}} > 0.05\,\max(v_{\mathrm{O}})$). This lag time was used as an index to characterize the timing of aromatic C degradation, while the temporal average of ligninolytic oxidation rate $\overline{v}_{\mathrm{O}}$ and the peak value of v_{O} (calculated as $\max(v_{\mathrm{O}})$) were used as indices of the aromatic C decomposition capacity.

We used linear mixed-effect models to disentangle the effects of climate and litter chemistry on aromatic C and litter decomposition rates. These models treated τ, v_{H}, r_{O}, $\max(v_{\mathrm{O}})$, and $\overline{v}_{\mathrm{O}}$ as response variables. The predictor variables were mean annual temperature (MAT), mean annual precipitation (MAP), initial litter C : N ratio (CN_0), initial aromatic C to litter N ratio, and the initial aromatic C. In the final model, we only used MAT, CN_0, and initial aromatic C to reduce collinearity among predictors. To enhance interpretability, all predictors were centered and scaled. Additionally, the data source was included as a random effect on the intercept to account for any study-specific variation. The Q_{10} temperature sensitivity values for hydrolytic and ligninolytic oxidation rates were estimated using fixed effect sizes of MAT from the linear mixed-effect model, and nonparametric bootstrapping was used to calculate confidence intervals.

All response variables were log-transformed to ensure the normality of residuals. Notably, the lag time τ exhibited a zero-inflated response. Therefore, we transformed it using $\log(\tau + K)$, where $K = 0.5\min(\tau > 0)$ was introduced to address instances where τ equaled zero. We also fitted τ using a zero-inflated generalized linear model from *glmmTMB* (Brooks *et al.*, 2017). However, here we only present results from the linear mixed-effect model because both resulted in similar significance levels for the predictors, and it is more straightforward to interpret coefficient estimates in linear models. The MATLAB *fitlme* function was used to perform these analyses.

Results

We start by presenting numerical explorations of model behavior (Figs 2, 3), followed by examples of model fitting (Fig. 4), model performance metrices (Fig. 5), and the results from the statistical analysis of how litter chemistry and climate affect model parameters (Figs 6, 7).

The first numerical exploration illustrates the temporal changes in total C remaining (red curves), aromatic C remaining (blue curves), and the optimal ligninolytic oxidation rate v_{O} (black curves) for different values of the time-invariant parameters hydrolytic rate v_{H}, cost of ligninolysis r_{O}, initial aromatic C, and necromass recycling into the aromatic C pool μ_{O} (Fig. 2). Our optimization approach predicted a temporally variable ligninolytic oxidation rate v_{O}. The optimal v_{O} was initially zero, but after a lag, it increased steeply, attained a maximum in the

New Phytologist

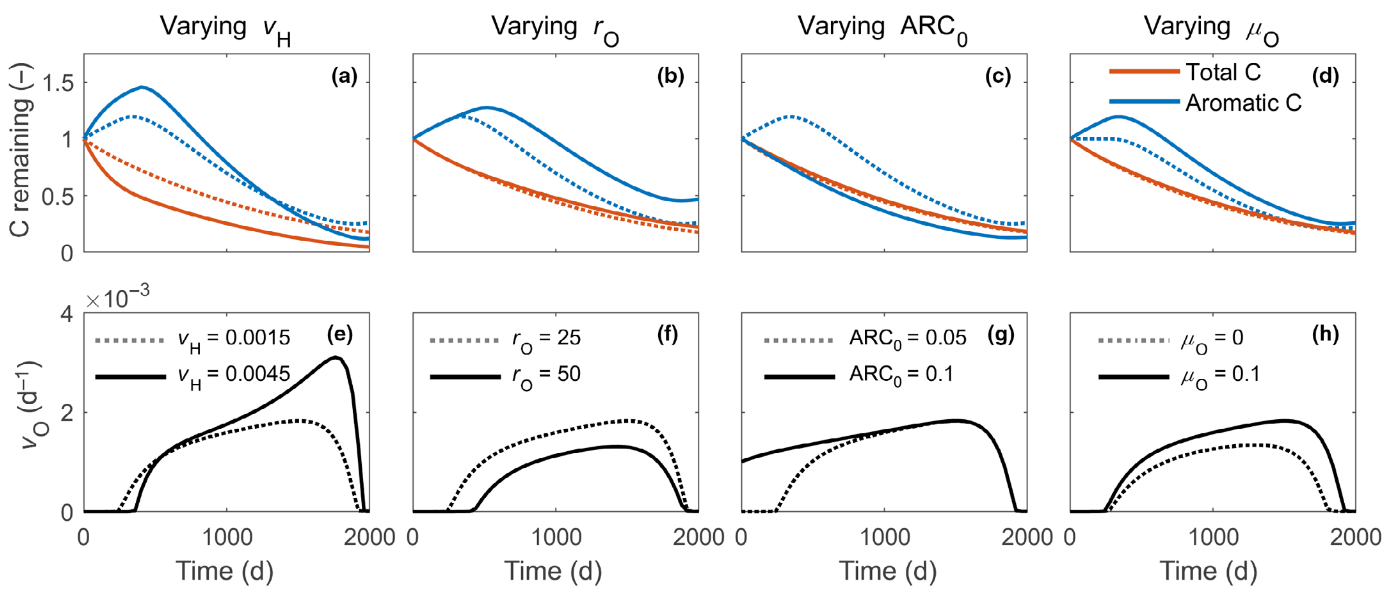

Fig. 2 Effect of the hydrolytic rate (v_H), cost of ligninolysis (r_O), initial fraction of aromatic C (ARC_0), and necromass cycling into the aromatic carbon (C) pool (μ_O) on (a–d) total litter C remaining and the aromatic C pool remaining, and (e–h) ligninolytic oxidation rate (v_O). Both C pools are expressed relative to the initial amounts. The dashed or solid lines denote low or high levels of the parameters being varied. Values of the fixed parameters in simulations are: $v_H = 0.0015\ d^{-1}$, $r_O = 25$ d, $\mu_O = 0.1$, $CN_0 = 50$, and $ARC_0 = 0.05$.

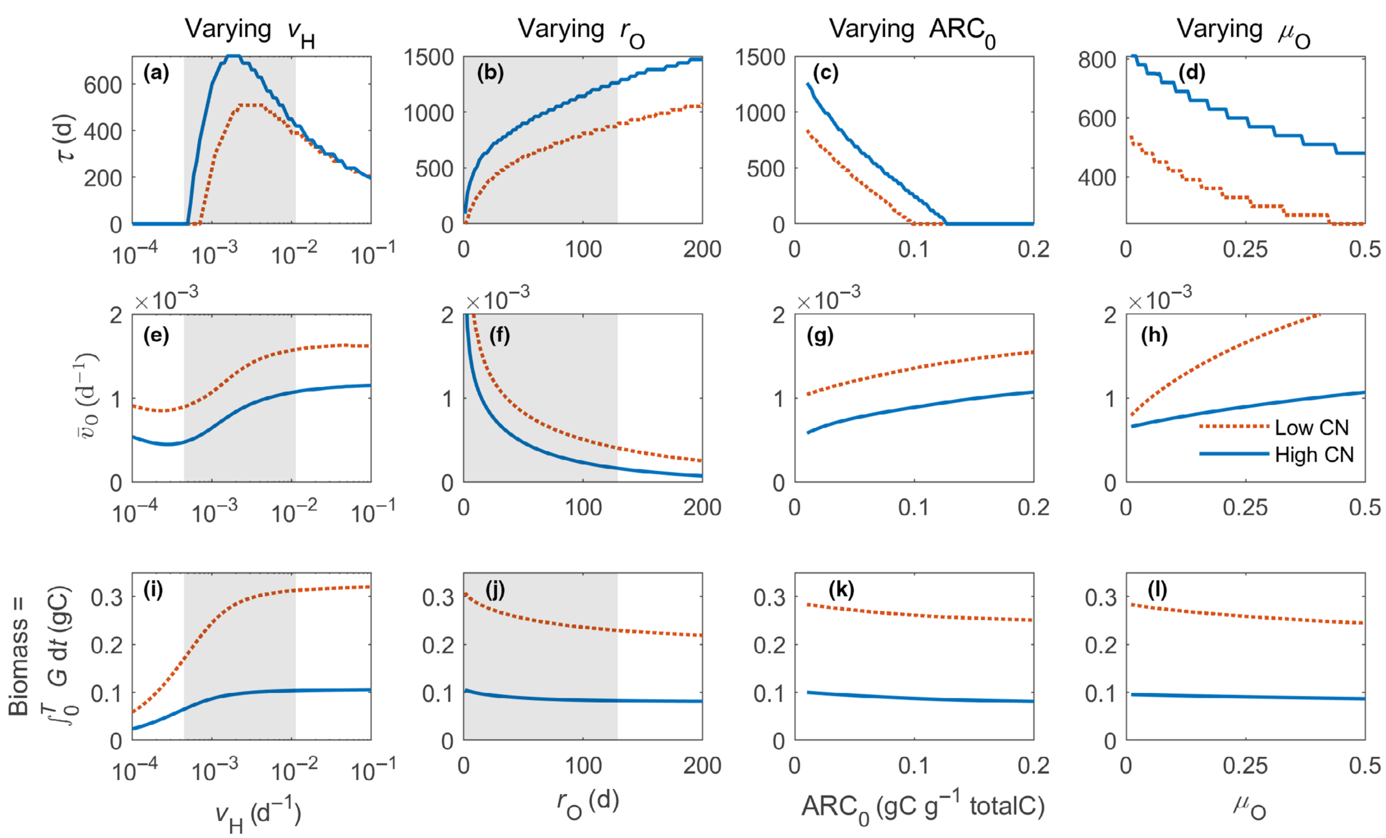

Fig. 3 Effect of the hydrolytic rate (v_H), cost of ligninolysis (r_O), initial fraction of aromatic carbon (C) (ARC_0), and necromass cycling into the aromatic C pool (μ_O) on (a–d) lag time of ligninolysis (τ), (e–h) temporal average of the ligninolytic oxidation rate ($\bar{v}_O$), and (i–l) cumulative microbial biomass growth. Values of the fixed parameters are: $v_H = 0.0015\ d^{-1}$, $r_O = 25$ d, $ARC_0 = 0.05$ gC g^{-1} litter, and $\mu_O = 0.1$. Red and blue lines represent low initial litter C : N ratio = 20 and high C : N ratio = 100, respectively. Mean rates are calculated from a fixed simulation period of 2000 d. The grey patch areas represent the observed range of estimated v_H and r_O.

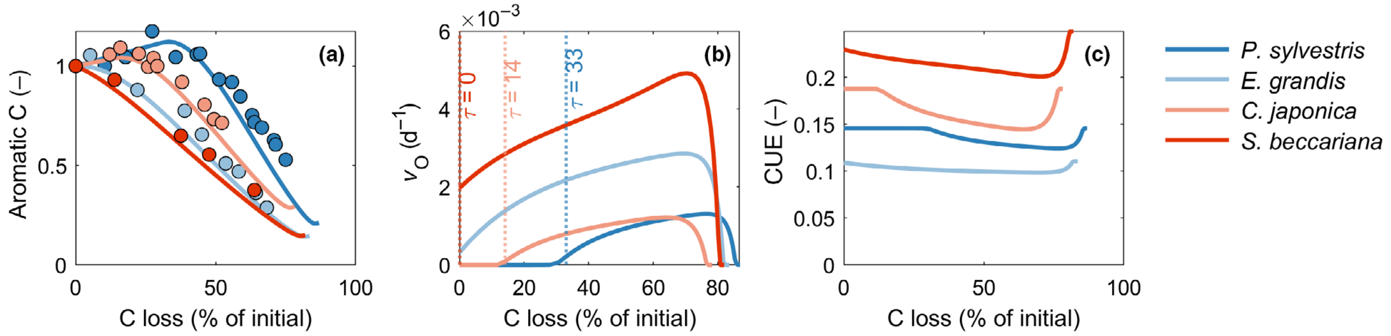

Fig. 4 Examples of model fitting: variation in (a) amount of aromatic carbon (C) normalized by the initial value, (b) ligninolytic oxidation rate (v_O), and (c) C-use efficiency, as a function of total C loss. Solid symbols represent observed ARC and total C loss measured at the same time points. Four litter types with contrasting initial aromatic C and initial C : N ratio from four different climates were chosen as examples–boreal: *Pinus sylvestris* L. leaves, $ARC_0 = 0.04$, $CN_0 = 132$, $r^2 = 0.96$, rmse = 0.05 from Berg & McClaugherty (1989), cold temperate: *Cryptomeria japonica* D. leaves, $ARC_0 = 0.08$, $CN_0 = 95$, $r^2 = 0.97$, rmse = 0.03 from Osono & Takeda (2005), warm temperate: *Eucalyptus grandis* H. twigs $ARC_0 = 0.06$, $CN_0 = 189$, $r^2 = 0.98$, rmse = 0.03 from Tu *et al*. (2014), and tropical: *Shorea beccariana B*. leaves, $ARC_0 = 0.1$, $CN_0 = 66$, $r^2 = 0.98$, rmse = 0.03 from Hirobe *et al*. (2004). Ligninolysis lag time (τ) values are in days.

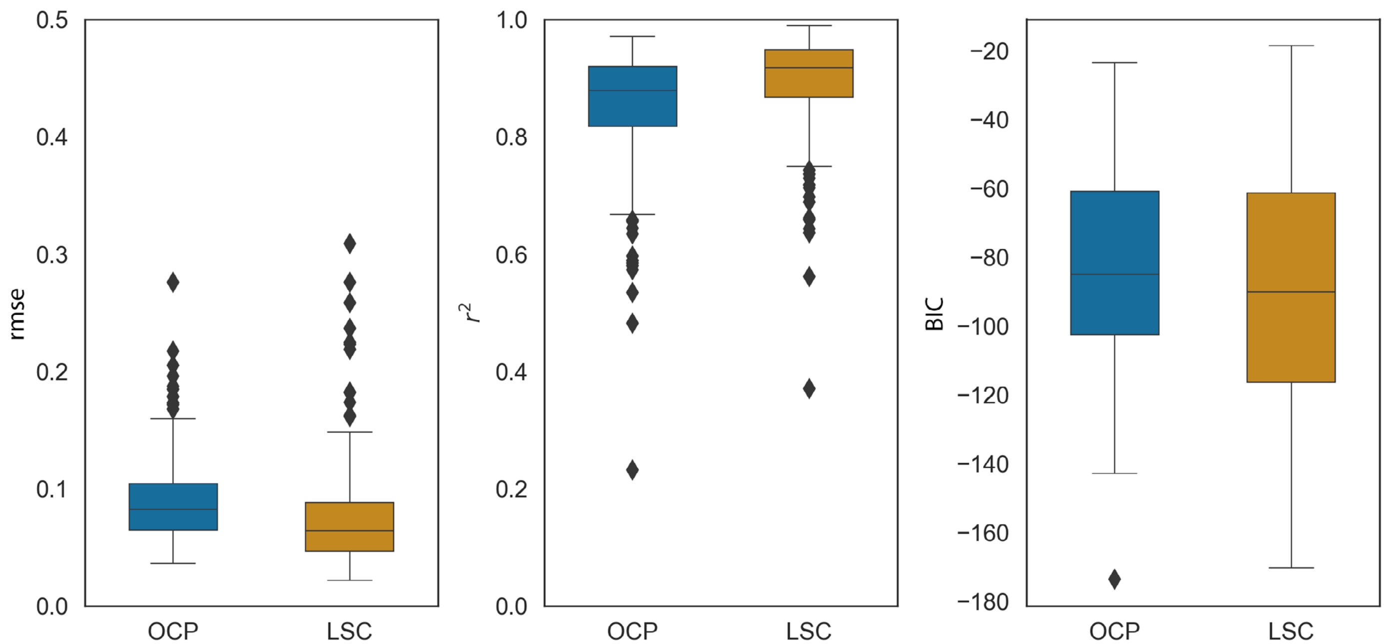

Fig. 5 Comparison of root mean squared error (rmse), coefficient of determination (r^2), and Bayesian information criterion (BIC) between optimal control model (OCP) and least-square fitting model (LSC). The ends of each box represent the 25th and 75th quantiles of rmse, r^2, and BIC, and the horizontal line within the box represents the median. Whiskers of each boxplot extend from the minimum and maximum values in 1.5 times interquartile range. Diamond points are outliers falling outside the whisker range.

intermediate phase of decomposition, and then decreased as the amount of C in both pools decreased. Increasing the hydrolytic rate v_H or the cost of ligninolysis r_O delayed decomposition of aromatic C, whereas increasing initial aromatic C or necromass recycling into the aromatic C pool μ_O reduced the lag time of ligninolysis. The lag time was most sensitive to initial aromatic C – a chemical trait that emerged as a key predictor also in the following analysis. A direct consequence of this temporal variation in optimal v_O is that the aromatic C can accumulate initially before ligninolysis starts or remain constant when v_O begins to increase but necromass recycling balances aromatic C decomposition. Aromatic C eventually decreases with rates similar to the whole litter C when v_O is sufficiently high (blue curves in Fig. 2). These different phases of the aromatic C trajectory vary not only according to v_O, but also depending on other model parameters.

Fig. 3 shows variation in three metrics that summarize the whole decomposition process: lag time of ligninolysis (τ, top row), temporal average of ligninolytic oxidation rate ($\overline{v}_O$, middle row), and cumulative microbial biomass growth (bottom row), as a function of other, time-invariant model parameters. As the rate of hydrolysis v_H was increased, the lag time remained close to zero for very low values of v_H and then peaked at intermediate

	MAT_S	$CN_{0,S}$	$ARC_{0,S}$	$MAT_S \times CN_{0,S}$	$MAT_S \times ARC_{0S}$	$CN_{0,S} \times ARC_{0,S}$	(r^2_{marg}, r^2_{cond})
$\log(\tau+K)$	−0.31±0.32 ns	−0.088±0.13 ns	−1.3±0.13***	−0.013±0.22 ns	0.53±0.12***	−0.69±0.27*	(0.31 , 0.79)
$\log(r_O)$	−0.46±0.22*	−0.045±0.093 ns	0.52±0.097***	0.14±0.16 ns	0.24±0.089**	−0.21±0.2 ns	(0.23 , 0.74)
$\log(v_H)$	0.31±0.095**	−0.28±0.037***	−0.16±0.039***	−0.26±0.064***	0.052±0.036 ns	0.023±0.078 ns	(0.37 , 0.82)
$\log(\bar{v}_O)$	0.3±0.17 .	−0.32±0.063***	−0.11±0.067 .	−0.38±0.11***	−0.13±0.061*	0.15±0.13 ns	(0.13 , 0.78)
$\log(\max(v_O))$	0.39±0.16*	−0.47±0.065***	−0.3±0.068***	−0.45±0.11***	−0.1±0.062 ns	0.25±0.14 .	(0.3 , 0.76)

Fig. 6 Estimates of fixed effects and their SE from linear mixed-effect models to predict ligninolysis lag time $\log(\tau + K)$, cost of ligninolysis $\log(r_O)$, the hydrolysis rate $\log(v_H)$, and temporal average and maximum of the ligninolytic oxidation rate, respectively $\log(\bar{v}_O)$, $\log(\max(v_O))$, as a function of mean annual temperature (MAT_S), initial C : N ratio ($CN_{0,S}$), initial fraction of aromatic carbon (C) ($ARC_{0,S}$), and their interaction terms as predictors. Red represents a negative relationship between response and predictor, green represents a positive relationship, and white represents an insignificant estimate. The rightmost column describes the marginal (r^2_{marg}) and conditional (r^2_{cond}) coefficients of determination. Subscript 'S' denotes that the predictors are scaled and centered to mean 0 and SD 1. Star symbols denote significance levels: ***, $P < 0.001$; **, $P < 0.01$; *, $P < 0.05$; ., $P < 0.1$, ns as not significant $P > 0.1$.

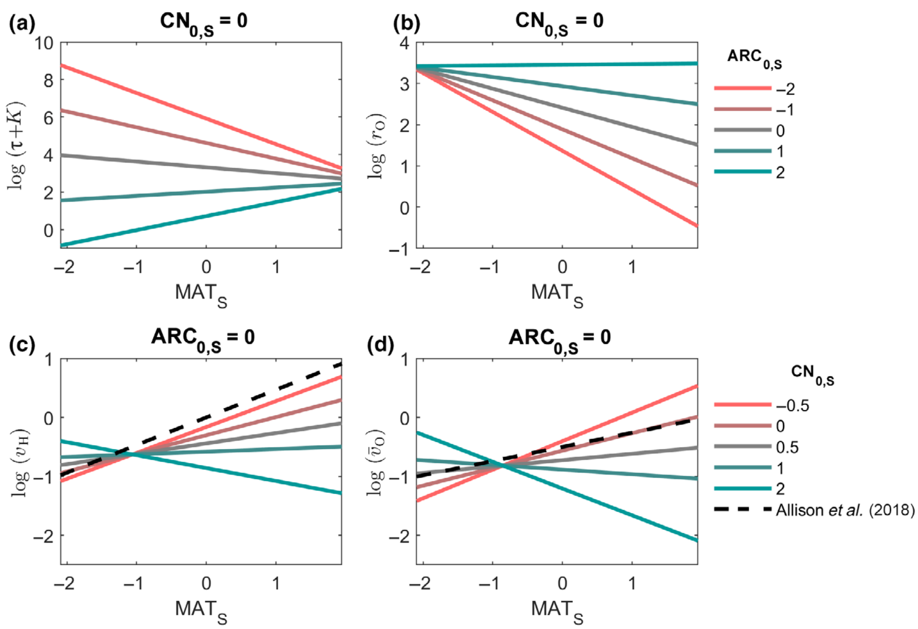

Fig. 7 Simulated variation of (a) ligninolysis lag time $\log(\tau + K)$, (b) cost of ligninolysis $\log(r_O)$, (c) hydrolysis rate $\log(v_H)$, and (d) temporal average ligninolytic oxidation rate $\log(\bar{v}_O)$ with changing mean annual temperature (MAT_S), initial C:N ratio ($CN_{0,S}$), and initial fraction of aromatic carbon (C) ($ARC_{0,S}$) using only the fixed effects from linear mixed-effect models. Note that for $\log(v_H)$ and $\log(\bar{v}_O)$ lines with different colors show variation with changing $CN_{0,S}$ and fixed $ARC_{0,S} = 0$, while for $\log(\tau + K)$ and $\log(r_O)$ lines with different colors show variation with changing $ARC_{0,S}$ and fixed $CN_{0,S} = 0$. Subscript 'S' denotes that the predictors are scaled and centered to have mean = 0 and SD = 1. The black dashed line in panels (c) and (d) denotes the average temperature sensitivity observed for hydrolytic and ligninolytic enzymes by Allison *et al*. (2018).

values of v_H (Fig. 3a). This implies that the decomposition of the aromatic C started immediately if the decomposition of nonaromatic C was not favorable (low values of $v_H \approx$ 1E-4 d^{-1}), resulting in a nonzero value of $\bar{v}_O$ (Fig. 3e). As the decomposition of nonaromatic pools became faster (increasing values of v_H, in the range of 1E-4 to 3E-4 d^{-1}), the rate of decomposition of the aromatic C was slightly reduced, but the lag time remained close to zero. However, for higher values of $v_H >$ 3E-4 d^{-1}, increasing v_H increased the $\bar{v}_O$ with a significant increase in lag time. For very high values of $v_H >$ 1E-2 d^{-1}, $\bar{v}_O$ remained stable.

Increasing the cost of ligninolysis r_O increased the lag time (Fig. 3b), while increasing initial aromatic C decreased it (Fig. 3c). Above a threshold of initial aromatic C *c*. 0.1 g aromatic C/g litter C, the lag time decreased to zero. Furthermore, increasing the fraction of necromass recycling into the aromatic C pool decreased the lag time (Fig. 3d) because having more C in the aromatic pool promotes its decomposition. Variation in average ligninolysis rate $\bar{v}_O$ followed opposite trends compared with lag time when increasing r_O, ARC_0, or μ_O (Fig. 3f–h).

The cumulative microbial biomass growth increased with increasing hydrolytic rate v_H, and decreased with increasing cost of ligninolysis r_O, initial aromatic C and necromass recycling into the aromatic C pool μ_O, although variations due to the last two factors were minor (Fig. 3i–l). These trends can be explained by the positive effect of nonaromatic C acquisition on growth, the negative effect of enzyme costs and litter recalcitrance, and the negative effect of recycling necromass in the aromatic C pool.

All metrics shown in Fig. 3 also depended on the initial litter C : N ratio (blue vs orange curves in Fig. 3), which was implemented via CUE in our model. A lower value of CN_0 implies lower N limitation, thus higher CUE and growth rate (dashed curves are all higher than the solid curves in Fig. 3i–l). Ultimately, higher CUE caused a larger fraction of decomposed C to be recycled as necromass, stimulating the decomposition of aromatic C (Fig. 3e–h) and decreasing lag time (Fig. 3a–d). Therefore, the effects of initial litter CN_0 on decomposition are all mediated by the feedback of CUE and growth on the dynamics of aromatic C.

In Fig. 4(a), four examples of least-square fitting of the model to total C and aromatic C loss data are shown. The selected data sets span different climates and initial litter quality to illustrate the range of behaviors in the data (and model output). The optimal ligninolytic oxidation rate v_O showed a similar pattern as in Fig. 2(e–h), with a peak of ligninolytic enzyme activity during late stages of decomposition, at *c.* 60–80% C loss (Fig. 4b). The estimated lag time was lowest ($\tau = 0$) in the *Shorea beccariana* litter, which had the highest initial aromatic C among the four litters; lag time was most delayed in the *Pinus sylvestris* litter, which had the lowest initial aromatic C (Fig. 4b). Furthermore, the CUE was lower in litter with higher CN_0, and decreased as decomposition proceeded because of ligninolysis costs (Fig. 4c). These examples are representative of the typical model performance, which was overall good, with r^2 generally higher than 0.8 and rmse lower than 0.1 g C/g initial C (Fig. 5). Notably, the two model variants – optimized v_O vs time-invariant v_O – performed similarly well (Fig. 5).

The results of the linear mixed-effect model used to identify the drivers of model parameters are shown in Fig. 6 (see also Figs S3, S4, S5; Table S1). The lag time of ligninolysis decreased with increasing initial aromatic C regardless of climate (Fig. 7a). It also decreased in warmer climates at low initial aromatic C, but increased in warmer climates at high initial aromatic C (Fig. 7a). The cost of ligninolysis r_O increased with increasing initial aromatic C and decreased in warmer climates, though temperature effects were most apparent at low initial aromatic C (Fig. 7b). The hydrolytic rate v_H increased in warmer conditions for low values of CN_0, but decreased for high CN_0 (Fig. 7c). The temporal average of the ligninolytic oxidation rate $\overline{v}_O$ followed the same patterns as v_H (Fig. 7d).

To compare the temperature sensitivities of hydrolytic and ligninolytic oxidation rates to observations, we used Q_{10} values reported by Allison *et al.* (2018). The temperature sensitivities of both v_H and $\overline{v}_O$ at low CN_0 were closer to the observed temperature sensitivities of hydrolytic and oxidative enzymes, respectively (black dashed lines in Fig. 7c,d). The Q_{10} values of the maximum ligninolytic oxidation (1.72 ± 0.16) rate were significantly higher than those of hydrolytic decomposition (1.53 ± 0.11) and the temporal average of ligninolytic oxidation (1.47 ± 0.26; Fig. S6). Furthermore, the Q_{10} of hydrolytic decomposition was significantly higher than the Q_{10} of the temporal average of ligninolytic oxidation (Tables S2, S3).

Discussion

Our litter decomposition model is based on an eco-evolutionary approach, assuming that ligninolysis is regulated to maximize the fitness of the microbial community. Using this model, we elucidated the effect of climate and litter quality on the decomposition rates of aromatic (lignin and other phenolics) and nonaromatic C compounds (soluble, cellulose, hemicellulose, proteins, and lipids). Here, we start discussing these results from a methodological perspective (Eco-evolutionary approach vs model with time-invariant rate parameters section); next, we focus on the patterns of ligninolytic oxidation (Simulated temporal patterns in optimal ligninolytic activity section); then, the chemical and climatic drivers are considered (Climate and litter quality controls ligninolysis section), and finally, a broad discussion on the application of eco-evolutionary principles in C cycling models is provided (Eco-evolutionary dynamics in carbon cycling models section).

Eco-evolutionary approach vs model with time-invariant rate parameters

Optimization approaches, such as the one proposed here, could help reduce the degrees of freedom (and related equifinality issues) of current, often over-parameterized models (Marschmann *et al.*, 2019; Harrison *et al.*, 2021). If optimization provides time-dependent model parameters, it can also capture the consequences of dynamic changes, such as alterations in enzyme production resulting from changes in microbial community composition as decomposition progresses. This possibility motivated our first question: whether the optimization model has higher predictive power than an alternate model with a time-invariant ligninolytic oxidation rate. We found that both models performed well, and their BIC values were similar, even though the model with time-invariant parameters has three fitting parameters and the optimization model has only two (Fig. 5). This indicates that the eco-evolutionary approach – substituting an unconstrained parameter with a maximization criterion (Eqn 5) – has equivalent performance as the more traditional model. This result is encouraging, as the optimization approach provides a framework informed by ecological theory that includes tradeoffs among microbial traits (here, ligninolytic capacity and C-use efficiency) and predicts temporal trait variation without requiring new observations for parametrization.

Simulated temporal patterns in optimal ligninolytic activity

Decomposition of the aromatic C pool increases the accessibility of protected cellulose and proteins, but low-molecular size products of complex aromatic polymers, such as lignin, can also actively enter metabolism to support microbial growth (del Cerro *et al.*, 2021). As a result, investment in ligninolytic enzymes might yield dual benefits. While some microbial explicit litter decomposition models have explored the effects of lignin-mediated carbohydrate protection on uptake rates and microbial C-use efficiency (Moorhead & Sinsabaugh, 2006; Manzoni *et al.*, 2021), none have investigated the emergent ligninolytic capacity that arises from maximizing cumulative growth rate. Our model capitalizes on the dual influences of the aromatic C pool, enabling us to predict optimal temporal variation in ligninolytic oxidation (v_O) during litter decay (Fig. 2).

Since v_O serves as a proxy for overall ligninolytic enzyme activity, a direct comparison with observed enzyme activities (e.g. peroxidase, laccase, or polyphenol oxidase) is not straightforward, because ligninolytic enzymes are multifaceted (Sinsabaugh, 2010) and several enzymes may act together to decompose aromatic compounds (Mori *et al.*, 2023; Schimel, 2023). Despite these methodological limitations, the simulated pattern of v_O was qualitatively similar to the activities of peroxidase and laccase enzymes reported in Huang *et al.* (2021) and Šnajdr *et al.* (2011; Fig. S7). The only notable difference between observations and model results was in the dataset by Huang *et al.* (2021), in which enzyme activity exhibited an early peak that our model could not predict. Such a peak is difficult to explain but is consistent with the early loss of lignin in that particular dataset. Overall, this independent evidence based on measured enzymatic activities lends additional support for the predicted decomposition patterns in the aromatic C pool.

Patterns in ligninolytic oxidation rate are explained by the controls of hydrolytic decomposition, cost of ligninolysis, and initial aromatic C, as these parameters combine the effects of climate, microbial metabolic tradeoff, and litter chemistry (Fig. 3). Depending on these parameters, the microbial community may initiate production of ligninolytic enzymes already in early stages of litter decay, or there might be a more or less long lag in ligninolytic activity leading to the often observed initial accumulation of aromatic C (Cotrufo *et al.*, 2015; Barbi *et al.*, 2020). When litter has a higher initial content of aromatic C, microorganisms prioritize the removal of the aromatic C to access the nonaromatic C, resulting in higher optimal rates of ligninolytic oxidation v_O and reduced lag time (Fig. 3c,g). However, microorganisms with a lower cost of ligninolysis, leading to higher CUE, can achieve higher growth rates, thereby facilitating increased investment in ligninolytic enzymes and subsequently increasing v_O (Fig. 3b,f). Notably, as the cost of ligninolysis is reduced, the initial aromatic C threshold level at which the lag time becomes zero is also lower (as illustrated in Fig. S8).

From the estimated parameters, we found a positive relation between hydrolytic and mean ligninolytic oxidation rates (see log (v_H) vs log$(\overline{v}_O)$ in Fig. S3; the range of these parameters is also illustrated as shaded areas in Fig. 3) – implying that faster hydrolysis is linked to faster ligninolysis. This coordination is particularly relevant in tropical forests, where warm and humid conditions prompt swift losses of labile litter pools, which in turn can increase losses of the more recalcitrant litter pool, thereby reducing the aromatic contribution to stable soil C. On the contrary, in cold climates and N-limited conditions, slow hydrolysis may lead to delayed aromatic C oxidation and accumulation of recalcitrant, aromatic residues. However, when hydrolytic C acquisition is very rapid (high v_H) or very slow (low v_H), the cumulative growth rate can only increase through decomposition of the aromatic pool, necessitating an early increase in v_O (i.e. short lag time; see Fig. 3a,e). In reality, forcing low v_H as we did in the numerical analysis of Fig. 3 might not be realistic, because hydrolytic enzymes are produced together with oxidative enzymes. High v_H is more likely to occur, and in that case it is reasonable to expect – as predicted by the model and estimated parameters – that ligninolytic capacity would also increase and start earlier during decomposition.

Climate and litter quality controls ligninolysis

We found that the lag time (τ) decreased, even though the predicted cost of ligninolysis (r_O) increased, with increasing initial aromatic C under all climatic conditions (red to green lines, Fig. 7a,b). This implies that microorganisms decomposing litter with higher initial aromatic C will invest early in ligninolytic enzymes because the benefits of accessing nonaromatic C outweigh the costs of ligninolysis. Furthermore, this effect was enhanced for N-poor litter (significant negative $ARC_0 \times CN_0$ term for τ in Fig. 6). By contrast, the average ligninolytic oxidation rate decreased at a higher initial C : N ratio, indicating that the average rate of aromatic C decomposition is slower in N-poor litter, consistent with findings by Talbot & Treseder (2012), who reported a decrease in lignin decay rate as litter C : N increased. Theoretically, in N-poor litter, decomposers may benefit if oxidation of aromatic litter components releases growth-limiting substrates, for example from protein–tannin complexes. Such mining for tightly bound N may be suppressed in N-rich litter (Craine *et al.*, 2007). Taken together, these results support the traditional hypothesis that microorganisms consume easily degradable C during the early stages of litter decay and later co-metabolize lignocellulose to access C and N from protected sugars and proteins (Berg & Staaf, 1980).

The effect of increasing temperature on lag time depended on initial aromatic C. The lag time decreased in warmer climates for high-quality litter (low initial aromatic C) but increased for low-quality litter (high initial aromatic C) due to the decreasing cost of ligninolysis with increasing temperature.

This study only included data on MAT, initial litter C : N ratio, and initial proportion of aromatic C, which explained 10–40% of the variance of the response variables. Other studies have reported that soil pH, fungal diversity and community composition, fungi-to-bacteria ratio, and soil minerals (e.g. Mn, Fe) correlate with aromatic C decomposition rates (Huang *et al.*, 2023). Here, we assumed that the effects of these potential predictors (for which we do not have complete data) are captured by including the data source as a random factor (which accounted for an additional 40–60% of the variance of the response variables, Table S1). In addition, our model does not account for microbial adaptation under conditions of N limitation or N excess, which could affect the relationship between ligninolytic oxidation and the C : N ratio of litter. We leave the development of such a model for a future contribution.

Warming accelerates microbial metabolism, but the sensitivity of decomposition rates to temperature also depends on other factors, such as substrate quantity and quality (Davidson & Janssens, 2006). We found that climate (MAT) and initial litter quality (initial aromatic C and C : N) together controlled the rates of hydrolysis (v_H) and ligninolytic oxidation ($\overline{v}_O$) and

$\max(v_O)$. The Q_{10} value of hydrolysis was higher than that of average ligninolytic oxidation, as also shown in empirical studies in litter (Nottingham *et al.*, 2016; Allison *et al.*, 2018; Tan *et al.*, 2020). However, the Q_{10} of maximum ligninolytic oxidation was even higher, suggesting that ligninolytic enzymes exhibit varying temperature sensitivity at different stages of litter decay (e.g. Duboc *et al.*, 2014). In soils, ligninolytic enzymes can have higher Q_{10} than hydrolytic enzymes (Davidson & Janssens, 2006; Wetterstedt *et al.*, 2010; Wang *et al.*, 2012), consistent with our results for maximum ligninolytic oxidation rate (Fig. 7).

Eco-evolutionary dynamics in carbon cycling models

The microbial engine that drives recycling of C and nutrients continuously adapts to the local conditions. For microbial systems, the evolutionary time scale is intermingled with ecological processes (changes in community composition), giving rise to eco-evolutionary dynamics at the community scale (Loreau *et al.*, 2023; Martiny *et al.*, 2023). These eco-evolutionary dynamics can feedback on soil C cycling in ways that are still not fully explored (Abs *et al.*, 2022). Here, we found wide ranges of estimated hydrolytic rates, cost of ligninolysis, and of the optimized temporal variation in ligninolytic oxidation rates, making a strong case against using fixed values of these parameters in soil and ecosystem models. Therefore, developing a framework accounting for adaptation of microbial resource acquisition strategies in a tractable manner that can be upscaled and integrated into a large-scale model is a much-needed advancement.

One major challenge in modelling microbial adaptation is the mathematical representation of eco-evolutionary dynamics governing the variation in parameters reflecting the plasticity of microbial functional traits in individual taxa, or the breadth of community composition variations driving community-level trait variation. Recent literature has proposed various mathematical approaches that employ optimality principles to elucidate optimal tradeoffs in organism life-history traits, thereby establishing a link between eco-evolutionary dynamics and shifting environmental conditions. For example, using an adaptive dynamics framework, Abs *et al.* (2022) showed that when tradeoffs between growth and extracellular enzyme production are accounted for, estimated losses of global C stocks increase. A simpler optimal control approach by Manzoni *et al.* (2023) showed that the optimal foraging strategy that maximizes microbial growth rate in a competitive environment favors high rates of resource uptake and low growth efficiency. These principles, rooted in optimizing resource allocation, extend beyond microbial systems and have been applied to plants (Feng *et al.*, 2022; Bassiouni *et al.*, 2023), underscoring their potential generality across diverse ecological contexts.

Conclusion

We developed a novel litter decomposition model based on an eco-evolutionary approach that maximizes mean microbial growth rate by finding the optimal ligninolytic activity. This model, constrained by >200 litter mass loss datasets, was used to assess the rate and starting time of decomposition of aromatic C (i.e. lignin and other phenolics) in plant litter. Climate and litter chemical quality interacted in controlling aromatic C decomposition. Specifically, warmer conditions accelerated decomposition rates, shortened the lag time of ligninolytic enzyme expression, and enhanced microbial C-use efficiency by reducing the predicted costs of ligninolysis. Furthermore, higher contents of aromatic C promoted its decomposition under any climatic conditions. We conclude that for a better understanding of aromatic C decomposition and stabilization in soil, it is crucial to consider interactions among climate, litter chemistry, and microbial metabolism. Eco-evolutionary approaches, such as the one proposed here, offer an avenue for capturing these interactions with less complex models that are easier to parameterize.

Acknowledgements

This project has received funding from the European Research Council (ERC) under the European Union's Horizon 2020 Research and Innovation Programme (grant no: 101001608), the Swedish Research Council Vetenskapsrådet (grant no: 2020-03910), and the Swedish Research Council FORMAS (grant no: 2021-02121). We thank T. Osono for sharing litter decomposition data, and A. Austin and three anonymous reviewers for their constructive comments.

Competing interests

None declared.

Author contributions

AC and SM conceived the study. AC developed the eco-evolutionary model and performed data fitting with feedback from SM and BDL. AC led the writing. All authors commented, reviewed, discussed the results, and contributed to the writing.

ORCID

Arjun Chakrawal https://orcid.org/0000-0003-4572-4347
Björn D. Lindahl https://orcid.org/0000-0002-3384-4547
Stefano Manzoni https://orcid.org/0000-0002-5960-5712

Data availability

Data and scripts used to analyze the data are available from doi: 10.5281/zenodo.10553503.

References

Abs E, Saleska S, Ferriere R. 2022. Microbial eco-evolutionary responses amplify global soil carbon loss with climate warming (preprint). In Review. doi: 10.21203/rs.3.rs-1984500/v1.

Allison SD, Romero-Olivares AL, Lu Y, Taylor JW, Treseder KK. 2018. Temperature sensitivities of extracellular enzyme Vmax and Km across thermal environments. *Global Change Biology* 24: 2884–2897.

Barbi F, Kohler A, Barry K, Baskaran P, Daum C, Fauchery L, Ihrmark K, Kuo A, LaButti K, Lipzen A *et al.* 2020. Fungal ecological strategies reflected in gene transcription – a case study of two litter decomposers. *Environmental Microbiology* 22: 1089–1103.

Baskaran P, Ekblad A, Soucémarianadin LN, Hyvönen R, Schleucher J, Lindahl BD. 2019. Nitrogen dynamics of decomposing Scots pine needle litter depends on colonizing fungal species. *FEMS Microbiology Ecology* 95: fiz059.

Bassiouni M, Manzoni S, Vico G. 2023. Optimal plant water use strategies explain soil moisture variability. *Advances in Water Resources* 173: 104405.

Berg B, McClaugherty C. 1987. Nitrogen release from litter in relation to the disappearance of lignin. *Biogeochemistry* 4: 219–224.

Berg B, McClaugherty C. 1989. Nitrogen and phosphorus release from decomposing litter in relation to the disappearance of lignin. *Canadian Journal of Botany* 67: 1148–1156.

Berg B, McClaugherty C. 2014. *Plant litter: decomposition, humus formation, carbon sequestration, 3rd edn.* Berlin, Heidelberg, Germany: Springer.

Berg B, Staaf H. 1980. Decomposition rate and chemical changes of Scots pine needle litter. I. Influence of stand age. *Ecological Bulletins* 32: 363–372.

Bhatnagar JM, Peay KG, Treseder KK. 2018. Litter chemistry influences decomposition through activity of specific microbial functional guilds. *Ecological Monographs* 88: 429–444.

Bonanomi G, Incerti G, Giannino F, Mingo A, Lanzotti V, Mazzoleni S. 2013. Litter quality assessed by solid state 13C NMR spectroscopy predicts decay rate better than C/N and Lignin/N ratios. *Soil Biology and Biochemistry* 56: 40–48.

Brooks ME, Kristensen K, Benthem KJ, van Magnusson A, Berg CW, Nielsen A, Skaug HJ, Mächler M, Bolker BM. 2017. Getting started with the GLMMTMB package. *R Journal* 9: 378.

Buresova A, Kopecky J, Hrdinkova V, Kamenik Z, Omelka M, Sagova-Mareckova M. 2019. Succession of microbial decomposers is determined by litter type, but site conditions drive decomposition rates. *Applied and Environmental Microbiology* 85: e01760-19.

Calabrese S, Mohanty BP, Malik AA. 2022. Soil microorganisms regulate extracellular enzyme production to maximize their growth rate. *Biogeochemistry* 158: 303–312.

del Cerro C, Erickson E, Dong T, Wong AR, Eder EK, Purvine SO, Mitchell HD, Weitz KK, Markillie LM, Burnet MC *et al.* 2021. Intracellular pathways for lignin catabolism in white-rot fungi. *Proceedings of the National Academy of Sciences, USA* 118: e2017381118.

Chen J, Elsgaard L, van Groenigen KJ, Olesen JE, Liang Z, Jiang Y, Lærke PE, Zhang Y, Luo Y, Hungate BA *et al.* 2020. Soil carbon loss with warming: new evidence from carbon-degrading enzymes. *Global Change Biology* 26: 1944–1952.

Cotrufo MF, Lavallee JM. 2022. Chapter One – Soil organic matter formation, persistence, and functioning: a synthesis of current understanding to inform its conservation and regeneration. In: Sparks DL, ed. *Advances in agronomy.* Amsterdam, the Netherlands: Elsevier, 1–66.

Cotrufo MF, Soong JL, Horton AJ, Campbell EE, Haddix ML, Wall DH, Parton WJ. 2015. Formation of soil organic matter via biochemical and physical pathways of litter mass loss. *Nature Geoscience* 8: 776–779.

Coûteaux MM, McTiernan KB, Berg B, Szuberla D, Dardenne P, Bottner P. 1998. Chemical composition and carbon mineralisation potential of Scots pine needles at different stages of decomposition. *Soil Biology and Biochemistry* 30: 583–595.

Craine JM, Morrow C, Fierer N. 2007. Microbial nitrogen limitation increases decomposition. *Ecology* 88: 2105–2113.

Dao TT, Mikutta R, Sauheitl L, Gentsch N, Shibistova O, Wild B, Schnecker J, Bárta J, Čapek P, Gittel A *et al.* 2022. Lignin preservation and microbial carbohydrate metabolism in permafrost soils. *Journal of Geophysical Research: Biogeosciences* 127: e2020JG006181.

Davidson EA, Janssens IA. 2006. Temperature sensitivity of soil carbon decomposition and feedbacks to climate change. *Nature* 440: 165–173.

Duboc O, Dignac M-F, Djukic I, Zehetner F, Gerzabek MH, Rumpel C. 2014. Lignin decomposition along an Alpine elevation gradient in relation to physicochemical and soil microbial parameters. *Global Change Biology* 20: 2272–2285.

Feng X, Lu Y, Jiang M, Katul G, Manzoni S, Mrad A, Vico G. 2022. Instantaneous stomatal optimization results in suboptimal carbon gain due to legacy effects. *Plant, Cell & Environment* 45: 3189–3204.

Fernandez CW, Heckman K, Kolka R, Kennedy PG. 2019. Melanin mitigates the accelerated decay of mycorrhizal necromass with peatland warming. *Ecology Letters* 22: 498–505.

Fioretto A, Di Nardo C, Papa S, Fuggi A. 2005. Lignin and cellulose degradation and nitrogen dynamics during decomposition of three leaf litter species in a Mediterranean ecosystem. *Soil Biology and Biochemistry* 37: 1083–1091.

Fioretto A, Papa S, Curcio E, Sorrentino G, Fuggi A. 2000. Enzyme dynamics on decomposing leaf litter of *Cistus incanus* and *Myrtus communis* in a Mediterranean ecosystem. *Soil Biology and Biochemistry* 32: 1847–1855.

Fioretto A, Papa S, Pellegrino A, Fuggi A. 2007. Decomposition dynamics of *Myrtus communis* and *Quercus ilex* leaf litter: mass loss, microbial activity and quality change. *Applied Soil Ecology* 36: 32–40.

Hall SJ, Huang W, Timokhin VI, Hammel KE. 2020. Lignin lags, leads, or limits the decomposition of litter and soil organic carbon. *Ecology* 101: e03113.

Harrison SP, Cramer W, Franklin O, Prentice IC, Wang H, Brännström Å, de Boer H, Dieckmann U, Joshi J, Keenan TF *et al.* 2021. Eco-evolutionary optimality as a means to improve vegetation and land-surface models. *New Phytologist* 231: 2125–2141.

He M, Zhao R, Tian Q, Huang L, Wang X, Liu F. 2019. Predominant effects of litter chemistry on lignin degradation in the early stage of leaf litter decomposition. *Plant and Soil* 442: 453–469.

He W, Wu F, Yang W, Tan B, Zhao Y, Wu Q, He M. 2016. Lignin degradation in foliar litter of two shrub species from the gap center to the closed Canopy in an Alpine Fir Forest. *Ecosystems* 19: 115–128.

Herzog C, Hartmann M, Frey B, Stierli B, Rumpel C, Buchmann N, Brunner I. 2019. Microbial succession on decomposing root litter in a drought-prone Scots pine forest. *The ISME Journal* 13: 2346–2362.

Hirobe M, Sabang J, Bhatta BK, Takeda H. 2004. Leaf-litter decomposition of 15 tree species in a lowland tropical rain forest in Sarawak: dynamics of carbon, nutrients, and organic constituents. *Journal of Forest Research* 9: 347–354.

Huang W, Hammel KE, Hao J, Thompson A, Timokhin VI, Hall SJ. 2019. Enrichment of lignin-derived carbon in mineral-associated soil organic matter. *Environmental Science & Technology* 53: 7522–7531.

Huang W, Yu W, Yi B, Raman E, Yang J, Hammel KE, Timokhin VI, Lu C, Howe A, Weintraub-Leff SR *et al.* 2023. Contrasting geochemical and fungal controls on decomposition of lignin and soil carbon at continental scale. *Nature Communications* 14: 2227.

Huang X-L, Chen J-Z, Wang D, Deng M-M, Wu M-Y, Tong B-L, Liu J-M. 2021. Simulated atmospheric nitrogen deposition inhibited the leaf litter decomposition of Cinnamomum migao H. W. Li in Southwest China. *Scientific Reports* 11: 1748.

King D, Roughgarden J. 1982. Graded allocation between vegetative and reproductive growth for annual plants in growing seasons of random length. *Theoretical Population Biology* 22: 1–16.

Kirk TK, Farrell RL. 1987. Enzymatic "combustion": the microbial degradation of lignin. *Annual Review of Microbiology* 41: 465–501.

Kou L, Chen W, Zhang X, Gao W, Yang H, Li D, Li S. 2015. Differential responses of needle and branch order-based root decay to nitrogen addition: dominant effects of acid-unhydrolyzable residue and microbial enzymes. *Plant and Soil* 394: 315–327.

Leek V. 2016. *An optimal control toolbox for MATLAB based on CasADi.* Dissertation. Linköping, Sweden: Linköping University. [WWW document] URL https://urn.kb.se/resolve?urn=urn:nbn:se:liu:diva-130891 [accessed 30 August 2016].

Lenhart S, Workman JT. 2007. *Optimal control applied to biological models, 1st edn.* New York, NY, USA: Chapman and Hall/CRC.

Loreau M, Jarne P, Martiny JBH. 2023. Opportunities to advance the synthesis of ecology and evolution. *Ecology Letters* 26: S11–S15.

Magill AH, Aber JD. 1998. Long-term effects of experimental nitrogen additions on foliar litter decay and humus formation in forest ecosystems. *Plant and Soil* 203: 301–311.

Manzoni S, Čapek P, Mooshammer M, Lindahl BD, Richter A, Šantrůčková H. 2017. Optimal metabolic regulation along resource stoichiometry gradients. *Ecology Letters* 20: 1182–1191.

Manzoni S, Chakrawal A, Ledder G. 2023. Decomposition rate as an emergent property of optimal microbial foraging. *Frontiers in Ecology and Evolution* 11.

Manzoni S, Chakrawal A, Spohn M, Lindahl BD. 2021. Modeling microbial adaptations to nutrient limitation during litter decomposition. *Frontiers in Forests and Global Change* 4.

Manzoni S, Trofymow JA, Jackson RB, Porporato A. 2010. Stoichiometric controls on carbon, nitrogen, and phosphorus dynamics in decomposing litter. *Ecological Monographs* **80**: 89–106.

Marschmann GL, Pagel H, Kügler P, Streck T. 2019. Equifinality, sloppiness, and emergent structures of mechanistic soil biogeochemical models. *Environmental Modelling & Software* **122**: 104518.

Martiny JBH, Martiny AC, Brodie E, Chase AB, Rodríguez-Verdugo A, Treseder KK, Allison SD. 2023. Investigating the eco-evolutionary response of microbiomes to environmental change. *Ecology Letters* **26**: S81–S90.

Mattila H, Österman-Udd J, Mali T, Lundell T. 2022. Basidiomycota fungi and ROS: genomic perspective on key enzymes involved in generation and mitigation of reactive oxygen species. *Frontiers in Fungal Biology* **3**: 837605.

McKee GA, Soong JL, Caldéron F, Borch T, Cotrufo MF. 2016. An integrated spectroscopic and wet chemical approach to investigate grass litter decomposition chemistry. *Biogeochemistry* **128**: 107–123.

McLellan TM, Aber JD, Martin ME, Melillo JM, Nadelhoffer KJ. 1991. Determination of nitrogen, lignin, and cellulose content of decomposing leaf material by near infrared reflectance spectroscopy. *Canadian Journal of Forest Research* **21**: 1684–1688.

Méndez MS, Ballaré CL, Austin AT. 2022. Dose–responses for solar radiation exposure reveal high sensitivity of microbial decomposition to changes in plant litter quality that occur during photodegradation. *New Phytologist* **235**: 2022–2033.

Moorhead DL, Lashermes G, Sinsabaugh RL, Weintraub MN. 2013. Calculating co-metabolic costs of lignin decay and their impacts on carbon use efficiency. *Soil Biology and Biochemistry* **66**: 17–19.

Moorhead DL, Sinsabaugh RL. 2006. A theoretical model of litter decay and microbial interaction. *Ecological Monographs* **76**: 151–174.

Mori T, Rosinger C, Margenot AJ. 2023. Enzymatic C:N:P stoichiometry: questionable assumptions and inconsistencies to infer soil microbial nutrient limitation. *Geoderma* **429**: 116242.

Nottingham AT, Turner BL, Whitaker J, Ostle N, Bardgett RD, McNamara NP, Salinas N, Meir P. 2016. Temperature sensitivity of soil enzymes along an elevation gradient in the Peruvian Andes. *Biogeochemistry* **127**: 217–230.

Osono T. 2017. Leaf litter decomposition of 12 tree species in a subtropical forest in Japan. *Ecological Research* **32**: 413–422.

Osono T, Takeda H. 2005. Decomposition of organic chemical components in relation to nitrogen dynamics in leaf litter of 14 tree species in a cool temperate forest. *Ecological Research* **20**: 41–49.

Preston CM, Nault JR, Trofymow JA. 2009a. Chemical changes during 6 years of decomposition of 11 litters in some Canadian forest sites. Part 2. ^{13}C abundance, solid-state ^{13}C NMR spectroscopy and the meaning of "lignin". *Ecosystems* **12**: 1078–1102.

Preston CM, Nault JR, Trofymow JA, Smyth C, CIDET Working Group. 2009b. Chemical changes during 6 years of decomposition of 11 litters in some canadian forest sites. Part 1. elemental composition, tannins, phenolics, and proximate fractions. *Ecosystems* **12**: 1053–1077.

Preston CM, Trofymow JA. 2015. The chemistry of some foliar litters and their sequential proximate analysis fractions. *Biogeochemistry* **126**: 197–209.

Růžek M, Tahovská K, Guggenberger G, Oulehle F. 2021. Litter decomposition in European coniferous and broadleaf forests under experimentally elevated acidity and nitrogen addition. *Plant and Soil* **463**: 471–485.

Schimel J. 2023. Modeling ecosystem-scale carbon dynamics in soil: the microbial dimension. *Soil Biology and Biochemistry* **178**: 108948.

See CR, Fernandez CW, Conley AM, DeLancey LC, Heckman KA, Kennedy PG, Hobbie SE. 2021. Distinct carbon fractions drive a generalisable two-pool model of fungal necromass decomposition. *Functional Ecology* **35**: 796–806.

Shimizu M, Yuda N, Nakamura T, Tanaka H, Wariishi H. 2005. Metabolic regulation at the tricarboxylic acid and glyoxylate cycles of the lignin-degrading basidiomycete *Phanerochaete chrysosporium* against exogenous addition of vanillin. *Proteomics* **5**: 3919–3931.

Sinsabaugh RL. 2010. Phenol oxidase, peroxidase and organic matter dynamics of soil. *Soil Biology and Biochemistry* **42**: 391–404.

Šnajdr J, Cajthaml T, Valášková V, Merhautová V, Petránková M, Spetz P, Leppänen K, Baldrian P. 2011. Transformation of *Quercus petraea* litter: successive changes in litter chemistry are reflected in differential enzyme activity and changes in the microbial community composition. *FEMS Microbiology Ecology* **75**: 291–303.

Talbot JM, Treseder KK. 2012. Interactions among lignin, cellulose, and nitrogen drive litter chemistry–decay relationships. *Ecology* **93**: 345–354.

Tan X, Machmuller MB, Huang F, He J, Chen J, Cotrufo MF, Shen W. 2020. Temperature sensitivity of ecoenzyme kinetics driving litter decomposition: the effects of nitrogen enrichment, litter chemistry, and decomposer community. *Soil Biology and Biochemistry* **148**: 107878.

Thevenot M, Dignac M-F, Rumpel C. 2010. Fate of lignins in soils: a review. *Soil Biology and Biochemistry* **42**: 1200–1211.

Tu L, Hu H, Chen G, Peng Y, Xiao Y, Hu T, Zhang J, Li X, Liu L, Tang Y. 2014. Nitrogen addition significantly affects forest litter decomposition under high levels of ambient nitrogen deposition. *PLoS ONE* **9**: e88752.

Tu L-H, Hu H-L, Hu T-X, Zhang J, Liu L, Li R-H, Dai H-Z, Luo S-H. 2011. Decomposition of different litter fractions in a subtropical bamboo ecosystem as affected by experimental nitrogen deposition. *Pedosphere* **21**: 685–695.

Vivelo S, Bhatnagar JM. 2019. An evolutionary signal to fungal succession during plant litter decay. *FEMS Microbiology Ecology* **95**: fiz145.

Wang G, Post WM, Mayes MA, Frerichs JT, Sindhu J. 2012. Parameter estimation for models of ligninolytic and cellulolytic enzyme kinetics. *Soil Biology and Biochemistry* **48**: 28–38.

Wetterstedt JÅM, Persson T, Ågren GI. 2010. Temperature sensitivity and substrate quality in soil organic matter decomposition: results of an incubation study with three substrates. *Global Change Biology* **16**: 1806–1819.

Yue K, Peng C, Yang W, Peng Y, Zhang C, Huang C, Wu F. 2016. Degradation of lignin and cellulose during foliar litter decomposition in an alpine forest river. *Ecosphere* **7**: e01523.

Zhou S, Huang C, Han B, Xiao Y, Tang J, Xiang Y, Luo C. 2017. Simulated nitrogen deposition significantly suppresses the decomposition of forest litter in a natural evergreen broad-leaved forest in the Rainy Area of Western China. *Plant and Soil* **420**: 135–145.

Zosso CU, Ofiti NOE, Torn MS, Wiesenberg GLB, Schmidt MWI. 2023. Rapid loss of complex polymers and pyrogenic carbon in subsoils under whole-soil warming. *Nature Geoscience* **16**: 344–348.

Supporting Information

Additional Supporting Information may be found online in the Supporting Information section at the end of the article.

Fig. S1 Geographical coordinates of litter bag incubation sites in the database.

Fig. S2 Variation of aromatic C content estimated from NMR spectra of Scots pine litter in relation to the C content of its acid unhydrolyzable residues.

Fig. S3 Scatter plot of response and predictors in the linear mixed-effect model.

Fig. S4 Pearson correlation plot between response and predictor variables.

Fig. S5 Fixed effect estimates for ligninolysis lag time (τ) using a generalized linear mixed effect with zero inflation model using glmmTMB.

Fig. S6 Q_{10} estimates of hydrolytic and ligninolytic oxidation rates.

Fig. S7 Comparisons of simulated ligninolytic oxidation rate with observed ligninolytic enzyme activity.

Fig. S8 Variation of lag time with initial aromatic C content for varying values of the cost of ligninolytic enzyme production.

Table S1 Summary of linear mixed-effect model results for the response variables.

Table S2 Temperature sensitivity index Q_{10} and activation energy (E_A) of hydrolytic and ligninolytic enzymes.

Table S3 Pairwise *t*-test statistics for comparing the significance difference in Q_{10}.

Please note: Wiley is not responsible for the content or functionality of any Supporting Information supplied by the authors. Any queries (other than missing material) should be directed to the *New Phytologist* Central Office.

See also the Commentary on this article by Shao & Sulman, **243**: 825–827.